J. Physiol. (1983), **339**, *pp.* 615–630
With 7 text-figures
Printed in Great Britain

PASSIVE BIAXIAL MECHANICAL PROPERTIES OF ISOLATED CANINE MYOCARDIUM

BY LINDA L. DEMER* AND FRANK C. P. YIN†
From the Departments of Biomedical Engineering and Medicine†, Johns Hopkins Medical Institutions, Baltimore, MD 21205, U.S.A.*

(*Received 27 April 1982*)

SUMMARY

1. Excised sheets of canine myocardium were subjected to cyclic loading and unloading in the predominant fibre and cross-fibre directions to determine passive mechanical properties.

2. Myocardium under biaxial loading exhibits both non-linear elasticity and viscoelasticity with some strain-rate dependence in the position of the stress–strain relations, but very little rate dependence in the area enclosed by the loading and unloading portions of the stress–strain loops.

3. Fibre and cross-fibre directions demonstrate anisotropic behaviour, with both the degree and direction of the anisotropy being dependent upon the region of the heart from which specimens are obtained.

4. In the same specimen biaxial as compared with uniaxial loading yields different interpretations as to the material properties.

INTRODUCTION

The three-dimensional relationship (constitutive relationship) between the normalized forces (stresses) and deformations (strains) is the fundamental description, independent of geometry or size, of the mechanical properties of any material. Determination of myocardial constitutive relations in the intact heart is particularly difficult because of our current inability to measure the forces accurately (Huisman, Elzinga, Westerhof & Sipkema, 1980). Obtaining the full myocardial constitutive relations from measurements in the intact heart is unlikely to succeed without significant advances in our measurement capabilities. In addition, other complicating factors in the intact heart include complex geometry, large deformations, heterogeneity of architecture, history dependence and anisotropy (Rabinowitz, 1978; Olsen, Lee, Tyson, Maier, Davis, McHale & Rankin, 1981). For instance, whether anisotropy is an inherent property of the muscle fibres or is due to the variation of fibre orientation throughout the heart wall (Streeter, Spotnitz, Patel, Ross & Sonnenblick, 1969; Rabinowitz, 1978; Arts & Reneman, 1980) is difficult to ascertain from studies in the whole heart.

To date, our knowledge of the constitutive relations of heart tissue is scanty and is based almost exclusively upon results from uniaxial studies in excised papillary muscles or strips of ventricular trabeculae carnae. While one-dimensional studies have contributed to our understanding of some of the fundamental mechanisms

underlying cardiac mechanics, it should be emphasized that it is not warranted quantitatively or, even qualitatively, to extrapolate one-dimensional results to the intact heart. For instance, what is isometric in the one-dimensional case is not isometric in three-dimensions because the lateral edges of the tissue are not fixed but are free to deform. Since the vast majority of tissue in the heart is subjected to multiaxial loads it is quite likely that extrapolations based upon uniaxial data do not reflect the true stresses or strains in the heart wall accurately. Furthermore, from theoretical considerations, uniaxial data cannot be generalized to provide a three-dimensional constitutive relation (Fung, 1973*a*). Thus, in order to obtain the fundamental data necessary for determination of the three-dimensional mechanics of myocardium, it is necessary to determine myocardial properties under multiaxial loading conditions. Indeed, several recent publications have emphasized the need for determination of myocardial constitutive relations under multiaxial loading conditions (Mirsky, 1976; Fung, 1973*b*; Panda & Natarajan, 1977; Vinson, Gibson & Yettram, 1979; Bergel & Hunter, 1979; Moriarty, 1980; Yin, 1981). If one assumes tissue incompressibility, one can generalize two-dimensional test data to obtain the full three-dimensional constitutive relations (Green & Adkins, 1960; Fung, 1973*a*). Thus, it appears that initial efforts should be directed towards measurements of multiaxial forces and deformations in isolated tissue from which myocardial constitutive relationships can be derived more easily.

The purpose of the present study was to determine the passive two-dimensional stress–strain relationship of canine myocardial tissue. Specifically, superfused thin sheets of left ventricular tissue from various regions and at various locations through the wall of mongrel canine hearts were studied under a variety of biaxial and uniaxial conditions to ascertain the following: (1) the extent of viscoelasticity under biaxial loading, (2) the presence of and degree of anisotropy between fibre and cross-fibre directions, (3) the regional heterogeneity of material properties and (4) the specific differences between results of uniaxial and biaxial testing in the same specimen.

METHODS

Specimen preparation

Fresh hearts were obtained from forty-nine dogs (approximately 20 kg) anaesthetized with sodium pentobarbitone (30 mg/kg) or sodium thiopentone (11 mg/kg). Sodium heparin (2000 i.u.) was administered intravenously to inhibit formation of thrombi in the myocardial vessels prior to removal from the animal. After removal, the heart was immediately rinsed and immersed in ice-cold oxygenated saline for several minutes before sectioning.

Beginning from the epicardial surface, thin 1–2 mm thick planar sections from the left ventricular free wall were obtained by making successive tangential slices using a commerical motor-driven rotary blade. Epicardial specimens were not used because of the presence of large coronary vessels. Endocardial specimens were avoided because of the trabeculations. For later examination of the regional heterogeneity of properties, the site of origin of the slices was recorded. The slice beneath the epicardial surface was denoted an 'outer' slice, that above the endocardial surface an 'inner' slice. Typically these slices were obtained at a depth greater than 2 mm from their respective surfaces. Slices from the anterior and posterior left ventricular free wall and from the basal and apical halves (above and below the equator) were studied. To mark the specimen's original orientation in the heart a black ink reference grid, aligned with the plane of the valve rings, was stamped onto the cut surface before taking each slice. Every heart was cut in the same fashion, only one specimen was used from each heart, and the region to be tested on a given day was selected at random.

To minimize artifacts from the edges, deformations in the central portion of the specimen were

measured, from which the strains were calculated. Accurate estimation of the stress in the central region (see below) required that each specimen be of uniform thickness. Thickness variations within each specimen were minimized by selecting specimens according to the following procedure. First, gross estimation of uniformity was made by using only specimens which by visual inspection transmitted light uniformly. In those specimens which appeared uniform visually, direct measurements of tissue thickness at several locations were made using a non-contact method while the specimen was submerged under iced saline. In a shallow bath attached to the stage of a microscope (Nikon model SCB 102) each specimen was held flat against the bottom of the bath by suction through a fine-mesh screen. A 10× water-immersion lens and 10× eyepiece together with a calibrated focusing knob were used to focus onto the upper muscle surface. The horizontal mechanical stage was then moved to measure another area of the tissue. The amount of adjustment required to re-focus onto the surface was presumed to relate directly to any variation in specimen thickness. The resolution of this measurement system was 35–40 μm. A minimum of nine different, widely spaced regions was measured to assess the thickness variation in each specimen. Only those specimens with less than 10% variation in thickness were considered suitable for testing.

The specimen was placed in a specially designed Plexiglas frame while its edges were prepared for mounting onto the test apparatus. During this stage of preparation the specimen was continuously superfused with a drip of iced Tyrode solution. To distribute the force more evenly along the edges and minimize damage from silk tearing through the tissue, stainless-steel hypodermic needles (Yale-Becton Dickinson, 25 gauge, 2 in.) were inserted along four edges of the tissue to form an approximately 3 × 3 cm square that was aligned with its edges parallel and perpendicular to the predominant fibre direction which could be determined from visual inspection of the specimen. The forces from the pulling arms of the apparatus were transferred to each edge of the tissue by four parallel arrays of sutures (size 5–0, black, braided silk). Each array was formed from one continuous strand which was looped nine times at evenly spaced intervals along the support needle (see inset of Fig. 1). The other end of each array was attached to the pulling arms of the apparatus. This method was chosen because it provided both fairly uniform force distribution and a minimum of tissue damage. Vertical movements of the specimen were minimized by attaching stryrofoam to the free ends of the support needles allowing the specimen to float in the bath.

To minimize edge effects, deformations for calculation of tissue strains were measured in the central one-third of the specimen using a video tracking system that has been described previously (Yin, Tompkins, Peterson & Intaglietta, 1972). To allow the tracking system to operate, a high contrast target is required. We found that demarcating the central region of the specimen with four strips (9 × 2 mm) of black carbon paper in a 1 cm square provided a suitable target for the dimension analyser. The strips were attached to the tissue surface with a single small dot of cyanoacrylate at the middle of each strip. After the tissue was prepared in this manner, which took 1·5–3 hr from the time of removal from the animal, the specimen was placed into the test chamber where the specimen was allowed slowly to reach its study temperature of 30 °C.

Apparatus

A schematic drawing of the apparatus is shown in Fig. 1*A*. The edges of the specimen were stretched by the outward movement of four pulling arms, oriented along two mutually perpendicular axes. Each pair of pulling arms rode on carriages connected to a common threaded rotating shaft. One arm was fixed solidly to its carriage while the other could rotate freely about a horizontal pivot. The primary threaded shaft was driven by a reversible, variable-speed motor (Harvard Apparatus), allowing the arms to separate at rates of 0·025–2·5 mm/sec. The second shaft was coupled to the first by a gear, chain and pulley mechanism. The ratio of the pulling rates in the two axes could be varied but only equal rates were used in this study. Uniaxial loading could be accomplished by disengaging the gear and pulley mechanism.

Coupling between the pulling arms and the tissue was accomplished via the thread array which was looped over a horizontal rod on the upper end of each arm (Fig. 1*B*). Forces along the axes were measured by two force transducers (Konigsberg model F5-A) with temperature-compensated instrumentation amplifiers (Konigsberg, model S1-2). The lower edge of the pivotted arms contacted the head of the force transducer as shown in Fig. 1*C*. Thus, forces in the thread array applied a moment at the upper end of the pivot arm, causing the lower end to apply a compressive force against the force transducer. The transducer head and outer face of the 'rotating' arm were adjusted to just contact at zero force; thus, tension on the thread array resulted only in transfer of force, not rotation.

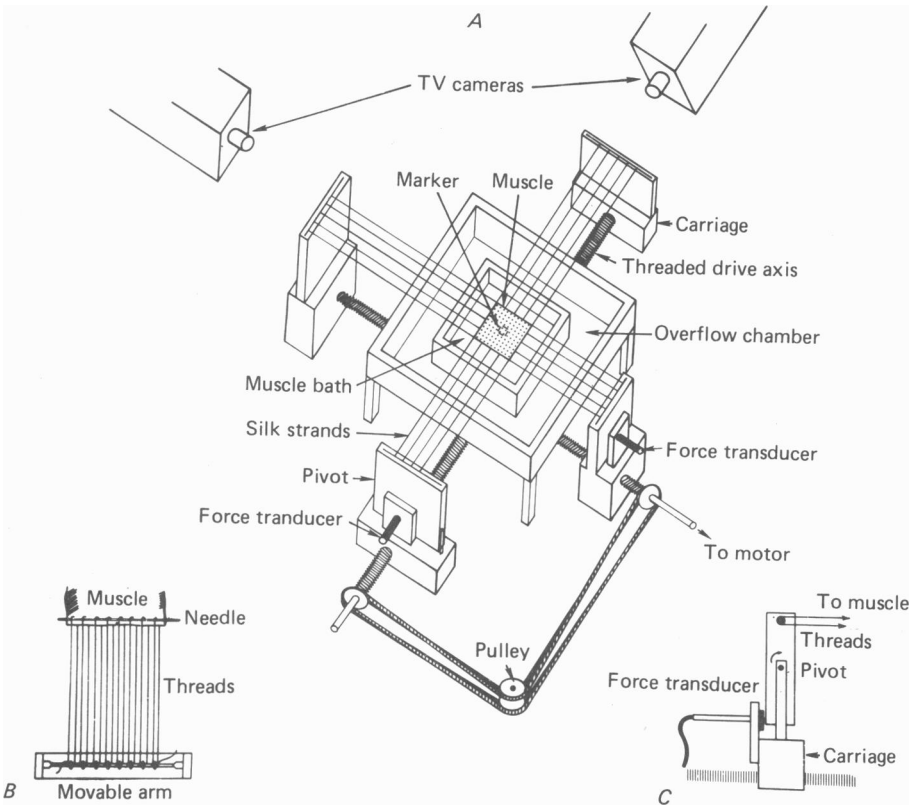

Fig. 1. *A*, schematic illustration of the experimental apparatus viewed from above. The tissue specimen is shown in the centre of the bath along with the four arrays of parallel threads connecting the specimen to the two orthogonal pairs of pivotted arms which ride on two orthogonal drive screws. The drive screws are coupled by the pulley and chain. The two pairs of sonomicrometer crystals used to measure the outer dimensions of the tissue between the ends of the thread arrays are now shown. The small central target on the specimen demarcates the central region in which the deformations are tracked by the two video cameras which are connected to video analysers (not shown) that produce voltages proportional to the distances between the target borders. Also not shown are the mirror and beam splitter which are mounted above the specimen. *B*, detail of one tissue edge illustrating the method of mounting the tissue to the loading arms. The movable arm is that which is located on the top of the pivotted head shown in a side view in *C*. The pivot provides a moment which transmits the force from the tissue to the transducers.

The images of the central target on the specimen passed through a beam splitter (Edmund Scientific, 40 mm) and a mirror (Melles-Griot, Inc.) to two mutually perpendicular silicon diode television cameras (model 4410 Cohu Instruments, San Diego, CA) which were supported horizontally above the bath. The images were displayed on Hitachi–Denshi Model VM 910 monitors. Illumination was achieved with a cold light, fibre-optic source (Dolan Jenner, Series 180). The two resulting video signals were processed using two Video Dimension Analysers (Model 303, Instrumentation for Physiology and Medicine, San Diego, CA) that produced two analogue voltages proportional to the distance between the mutually orthogonal pairs of markers as previously described (Yin *et al.* 1972).

In order to calculate stresses acting in the central region, where the deformations were measured, it was necesary to measure the dimensions of the tissue between the needles where the forces were exerted. These dimensions were measured by two pairs of piezoelectric crystals fitted with epoxy

lenses (Scheussler and Associates, Biomedical Instrumentation, Del Mar, CA) activated by a custom-built four-channel sonomicrometer which produced signals proportional to the instantaneous distance between the two opposite edges of the specimen. Proper triggering of the sonomicrometer was assured by continuous monitoring of the transmitted and received signals on a storage oscilloscope (Tektronix 5441, Beaverton, OR). The crystals were mounted on the ends of four Plexiglas bars extending from the movable carriages of the loading apparatus in a fixed relationship to the needles, thereby allowing determination of the instantaneous distance between the needles.

Protocol

Throughout the study, the specimen was floated in Tyrode solution of the following composition (mM): Na, 150; K, 3·0; Cl, 143; PO_4, 0·6; Ca, 2·6; Mg, 1·0; HCO_3, 12; glucose, 10. The solution was freshly prepared at the start of each study and was bubbled with 95 % O_2 and 5 % CO_2 to maintain pH at 7·4. Temperature in the test chamber was maintained at 29·5–30·5 °C by use of a thermistor (Cole-Parmer 8502-50) and heat exchanger (Travenol 5M0337) connected to a circulating water bath (VWR Scientific Inc., San Francisco, CA).

All specimens were initially pre-conditioned (Fung, 1967, 1973*a*) by simultaneously biaxially loading and unloading the specimen between nominal forces of about 1–200 g at an intermediate stretch rate (0·0125 mm/sec as measured in the central region). The first pre-conditioning cycle was quite different from the later cycles, but subsequent cycles became more reproducible. Preliminary checks showed that eight cycles over a 30 min period sufficed to produce reproducible force–deformation loops. On average, nine pre-conditioning cycles were used before data were collected. After pre-conditioning the tissue was unloaded to 1 g force along each edge. The dimensions under this condition constituted the reference from which the subsequent stretch ratios were calculated.

The biaxial tests were performed with one axis aligned along the predominant fibre direction and the second axis perpendicular to the fibre direction (cross-fibre). The following four loading conditions were studied.

(*a*) Biaxial: loading and unloading were performed at constant and equal rates.

(*b*) Isometric uniaxial: loading and unloading were performed in one axis while the outer dimensions in the other direction were held approximately constant.

(*c*) Constrained uniaxial: loading and unloading were performed in one direction while the edges of the opposite direction were free to move with the support needles left in place.

(*d*) Unconstrained uniaxial: one axis was loaded and unloaded while the other edges were free to move with the support needles removed.

Each of the protocols (*a*)–(*d*) were conducted at rates of 0·0025, 0·025, 0·1 and 0·25 mm/sec as measured in the central region. The tissue was then rotated 90° in the test chamber and the tests were repeated. At the end of the study both the tissue within the needle borders as well as in the central region were weighed, after light blotting, on a scale reading to 0·005 g. Average thickness for each specimen was determined by assuming a muscle density of 1·06 g/cm^3.

Data analysis

Prior to each study linearity checks and calibration of the force transducers, sonomicrometers, and video dimension analysers were performed. During the study the forces along each outer edge, the outer edge dimensions, and the central region dimensions were recorded on analogue tape for subsequent analysis (Hewlett-Packard 3968A, Waltham, MA).

Two force signals and the two inner region length signals were amplified using adjustable gain/adjustable offset operational amplifiers. All four length signals were low-pass filtered (30 Hz cut-off) to remove a small amount of 60 Hz noise before analogue-to-digital conversion with a twelve-bit convertor on a Data General S-130 minicomputer. The data were digitized so that each loading and unloading phase consisted of between 200–1000 points.

From these digitized data, the Eulerian stresses (force/instantaneous area) along the fibre and cross-fibre directions at the central region were calculated. In making these calculations we assumed that (1) the tissue was incompressible, (2) thickness was uniform and (3) forces were transmitted proportionally from the edges to the central region. The last assumption requires knowledge of the instantaneous dimensions between the needles and is the reason that the sonomicrometer data were required. The Eulerian strain (or stretch ratio) in the central region was calculated directly as the instantaneous length divided by the reference length. We assessed the presence and directionality of anisotropy qualitatively from computer generated plots of stress *versus* stretch ratio for the fibre *versus* cross-fibre directions for the protocol (a).

Because our apparatus did not allow us to feed-back control the central dimension independently, we could not perform a strictly isometric test in the protocol (b) as the orthogonal axis was being loaded. However, in order to obtain some quantitative information regarding the degree of anisotropy, we used the following method. We found eleven specimens in which the central region strains in the unloaded direction remained nearly isometric (less than a 2 % change in stretch ratio) as the opposite direction was loaded over its entire range. For each of the loaded axes, we fitted the stress–stretch ratio relationship to an exponential relationship of the form

$$\text{stress} = A \exp [B(\text{stretch ratio} - 1)] + C$$

using an iterative least-squares method (Dixon, 1981, pp. 290–303). The corresponding coefficients for the fibre and cross-fibre directions were compared.

RESULTS

Tracings of computer-generated plots from three sequential biaxial loading and unloading cycles performed after pre-conditioning are shown in Fig. 2. The ordinate is the stress in the fibre direction and the abscissa is the stretch ratio in the fibre direction. This Figure demonstrates several characteristic features seen in all of the tests. First, the highly reproducible results that can be obtained after pre-conditioning are evident. Secondly, the stress–stretch curve is highly non-linear. Thirdly, there is a large amount of hysteresis, i.e. the curves in loading and unloading are different. In every specimen the hysteresis loop was inscribed in a clockwise direction during the sequence of loading and unloading, respectively.

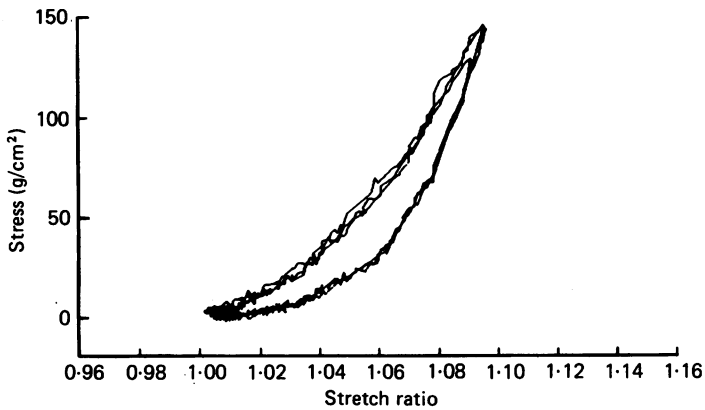

Fig. 2. Computer printouts of three consecutive loading and unloading cycles after completion of pre-conditioning. The axes have been redrawn for clarity.

In addition to hysteresis, which is one manifestation of viscoelastic behaviour, each specimen demonstrated stretch-rate dependence. A representative example of the rate dependence of the stress–stretch curve at the extremes of the rates employed is illustrated in Fig. 3. At a given stretch ratio, the stress was higher for faster rates of loading and unloading. This rate dependence is not striking, however, as there was only a moderate leftward shift of the stress–stretch curves despite a 100-fold increase in loading rate. It should be noted that the size of the hysteresis loops, which is an indication of the amount of energy dissipated by viscous losses in the loading and unloading process, demonstrated very little rate dependence.

Illustrative examples of the markedly different results that are obtained in the same specimen under biaxial compared to unconstrained uniaxial conditions are shown in Fig. 4 in which, for clarity, only the loading portions of the curves are shown. The ordinate is the stress and the abscissa is the stretch in the cross-fibre direction. Each number represents one specimen. In every case the tissue was stiffer under biaxial compared to uniaxial conditions.

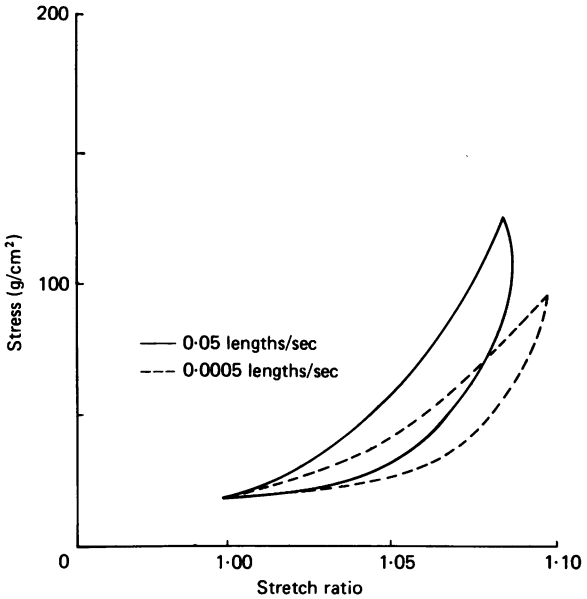

Fig. 3. Stress–stretch loops in the fibre direction under simultaneous biaxial loading and unloading. The strain rates for the two loops differed by 100-fold but there was relatively little stiffening of the tissue at the higher rate and very little difference in the area enclosed by the loops.

Further examples of the difference between uniaxial and biaxial test results are shown in Fig. 5. The results shown in the upper panel demonstrate nearly identical stress–stretch curves in the fibre and cross-fibre directions under biaxial loading, whereas under constrained uniaxial loading applied sequentially in the two directions the fibre direction appeared to be stiffer. The converse is shown in the lower panel of the Figure in which another specimen appeared to be stiffer in the fibre direction under biaxial loading whereas there was no difference when each direction was individually loaded.

Because of these differences between uniaxial and biaxial results, we used only the simultaneous, equal-stretch biaxial loading tests to assess the presence of anisotropy between fibre and cross-fibre directions. The presence of anistropy is evident when the mutually perpendicular stress–stretch curves of a given specimen are plotted on the same graph, as in Fig. 5. Since the stretch ratios in the two directions are nearly equal, each curve represents the 45° projection onto its stress–stretch plane. The relative stiffness in each direction can be ascertained by directly comparing the curves. When such comparisons were made for each specimen, we found that sixteen specimens were stiffer in the fibre direction, nineteen were stiffer in the cross-fibre

direction, and eleven specimens had negligible anisotropy. In those specimens that exhibited definite anisotropy, we used stepwise logistic regression analysis (Dixon, 1981, pp. 330–338) to assess the statistical significance of the regionality of anisotropy. When the region of origin of the specimen was taken into account, as summarized in Table 1, significantly more specimens from the outer, basal portion of the wall were stiffer in the cross-fibre compared to the fibre direction whereas significantly more specimens from the inner, apical portion of the wall were stiffer in the fibre direction ($P = 0{\cdot}05$).

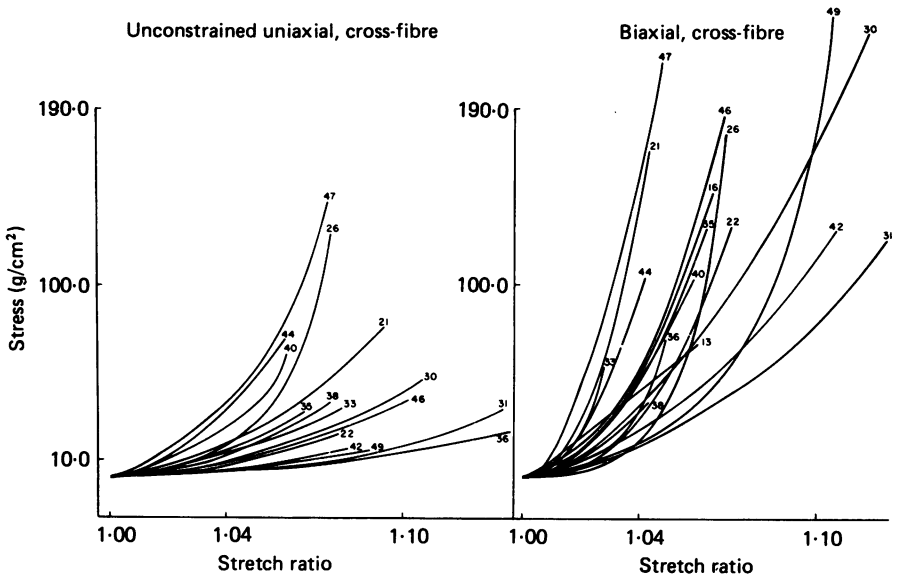

Fig. 4. Comparison of the loading portions of the stress–stretch curves in the cross-fibre direction during unconstrained uniaxial as compared with equal biaxial loading. The numbers identify each particular specimen which was subjected to both types of boundary conditions. In each instance the tissue was stiffer under biaxial as compared with uniaxial loading.

For the eleven specimens which remained nearly isometric along the unstretched axis during protocol (b), the numerically derived coefficients for the exponential relationship between stress and stretch ratio for both the fibre and cross-fibre directions are listed in Table 2. The exponential coefficient B primarily determines the stiffness of the stress–stretch ratio curve and is analogous to the exponential stiffness coefficient derived in uniaxial tests. This coefficient can differ by as much as a factor of two in the two directions. A graphical illustration of the stress–stretch ratio relationship for both the fibre and cross-fibre directions for one of the specimens listed in Table 2 is shown in Fig. 6.

DISCUSSION

Critique of the method

It has previously been shown that mechanical clamps used to mount cardiac tissue for *in vitro* testing produce damage near the ends of the muscle that introduce stray compliance into the system (Krueger & Pollack, 1975; Huntsman, Day & Stewart,

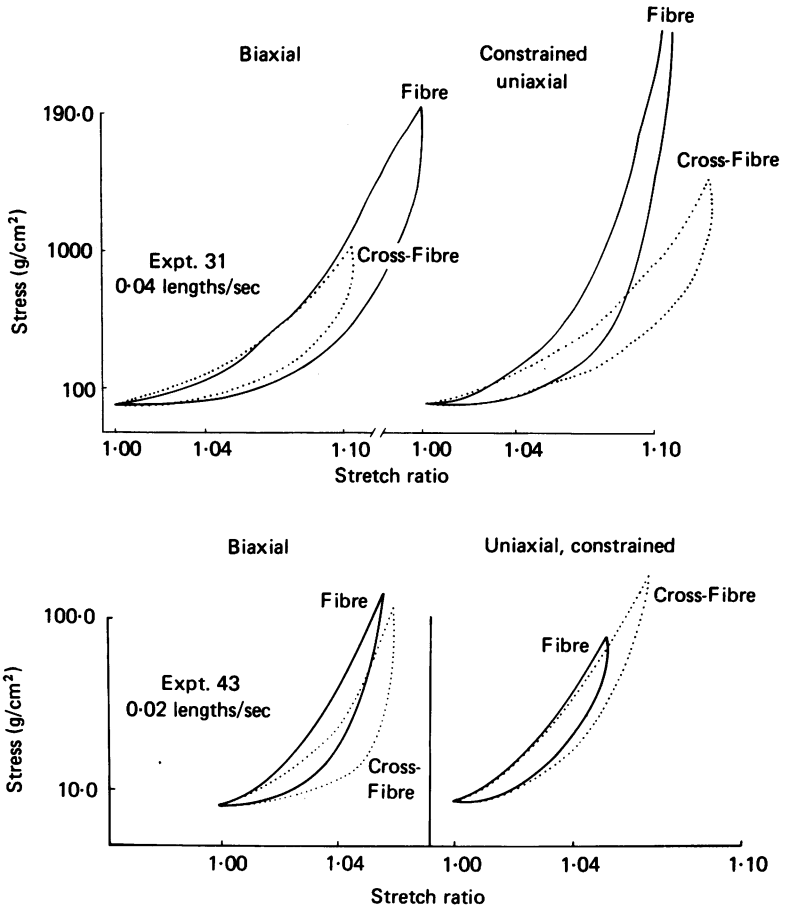

Fig. 5. Comparison of the different indications as to the presence and degree of anisotropy in the fibre as compared with the cross-fibre directions in biaxial and constrained uniaxial tests in the same tissue specimen. In the upper panel, the biaxial test indicates no anisotropy whereas two successive uniaxial tests indicate the fibre direction to be stiffer than the cross-fibre direction. In the lower panel, results from a different specimen show the converse.

TABLE 1. Regional dependence of relative stiffness between the fibre and cross-fibre directions in sheets of passive canine myocardium. Data represent the proportion of specimens that are relatively stiffer in the fibre compared to cross-fibre directions. Statistical analysis performed by stepwise logistic regression

Outer half of wall		Inner half of wall	
Apical	3/7	9/11	$P = 0{\cdot}05$
Basal	1/8	3/9	

1977). Therefore many systems have been devised to measure segment lengths near the central region of the tissue where damage effects are presumably minimized (Krueger & Pollack, 1975; Huntsman *et al.* 1977; Wiegner & Bing, 1979). Similarly, in the present study dimensional changes were measured in the central portion of the specimen. The mounting system for the edges of the tissue should, ideally, produce

TABLE 2. Coefficients for the exponential stress–stretch relations* in the fibre and cross-fibre directions under successive isometric uniaxial tests

	Fibre direction			Cross-fibre direction		
Specimen	(a)	(b)	(c)	(a)	(b)	(c)
310	24·20	13·11	−31·20	27·30	15·4	−26·90
317	11·60	25·50	−5·30	22·00	11·98	−21·12
318	95·07	16·28	−92·41	32·05	21·42	−28·86
324	65·30	10·89	−64·09	87·30	14·06	−86·75
407	26·15	23·12	−24·70	25·14	13·47	−28·64
422	43·66	25·87	−43·81	95·99	8·11	−93·22
423	128·70	6·57	−132·40	37·04	13·88	−39·77
602	2·03	28·51	−9·28	15·07	21·93	−8·96
609	31·50	22·50	−29·60	54·90	18·88	−56·30
623	32·65	25·41	−27·80	23·20	17·94	−19·21
701	25·30	31·60	−16·58	16·30	16·00	−2·76

* Stress–stretch relation of the form: stress = $A\exp[B(\text{stetch ratio}-1)]+C$.

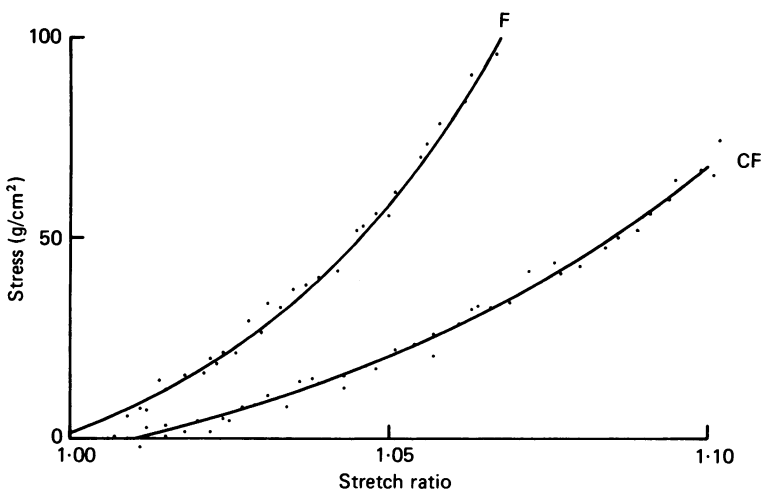

Fig. 6. Loading portions of the stress–stretch curves for the fibre (F) and cross-fibre (CF) directions of a specimen under two successive isometric uniaxial tests (symbols) with the specimen rotated 90° between tests. The lines are the results obtained from the exponential fit to the data. The coefficients for the exponential in each direction are listed in Table 2.

no tissue damage and also allow unrestrained lateral motion. In practice, we found that use of individual strands of silk, while allowing free lateral motion, often produced tears in the tissue. In addition it was also difficult to assure that there was equal tension in each strand. The system we chose after considerable testing was a compromise between these difficulties.

The use of a support needle undoubtedly produces some restraint to free lateral motion because of the friction between the tissue and the needle, but it did allow us to achieve high levels of passive force with no evidence of tears developing in the tissue. An example of the effect of lateral restraint is shown in Fig. 7. The upper panel compares results of the unconstrained and constrained uniaxial tests with the

latter demonstrating an apparently greater tissue stiffness at all strain rates. This difference, however, is due to both lateral restraint caused by presence of the needle as well as deformation of the unloaded edges as illustrated in the inset. To test directly for the effect of restraint due solely to the presence of the needle we performed another study in which deformation of the lateral edges with the needle removed was prevented. This was done by cutting the continuous thread array to make each loop independent. By adjusting the tension in each loop the edges could be held

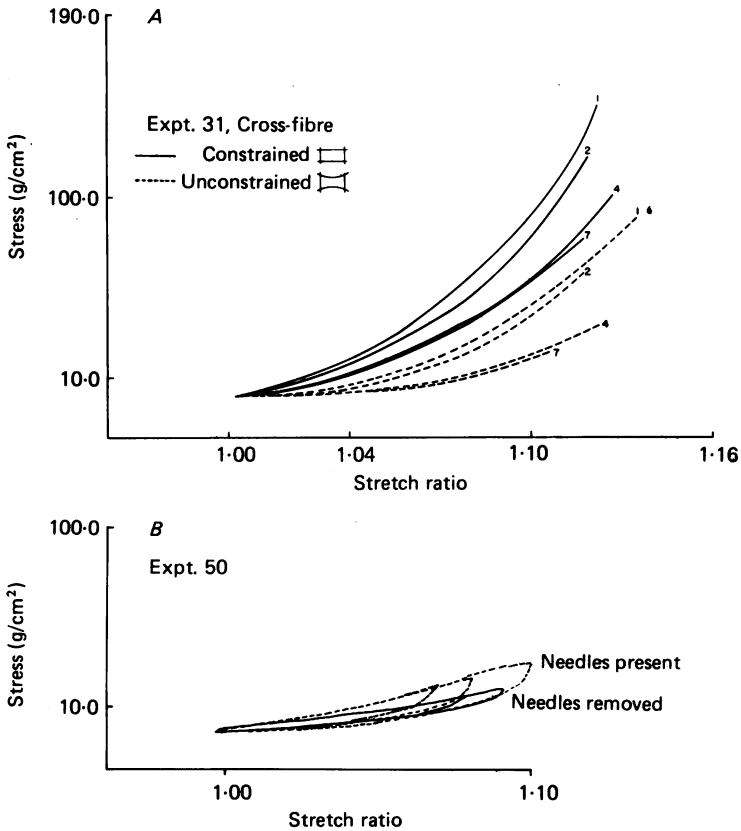

Fig. 7. *A*, comparison of the loading portion only of constrained and unconstrained uniaxial stress–stretch curves in the cross-fibre direction at the four strain rates used. Curve 1: 0·25 mm/sec; curve 2: 0·1 mm/sec; curve 4: 0·025 mm/sec; curve 7: 0·0025 mm/sec. *B*, comparison of stress–stretch curves in the cross-fibre direction with and without the support needles in place. When the needles were removed, the thread array was cut and the edges of the specimen were kept as nearly undeformed as possible by continually adjusting the tension in each strand as the tissue was loaded in the orthogonal direction.

approximately at the undeformed position. When this was done the results in the lower panel of the Figure were obtained. These results show that there is a small but definite effect of the needle on tissue stiffness. Hence, the absolute values of stiffness are likely over-estimations. However, since the needles were placed in both the fibre and cross-fibre directions in the results reported, the qualitative conclusions regarding anisotropy are probably still valid.

Use of the continuous strand of silk allowed us more nearly to equalize the tension between the individual loops. The frictional force produced by the silk passing through the tissue and over the pulling rod was found to be about 2 g, so that we can be reasonably certain that the tension between adjacent loops differed by no more than this amount. It is difficult to equalize tension even to this degree when individual strands are used. This unequal tension not only causes non-uniform force distribution, but also produces distortion along the edges of the tissue, causing local shearing whose effects may be transmitted to the interior regions of the specimen.

In uniaxial specimens the stress acting on the region where the segment length is measured can be reasonably estimated by dividing the uniaxial force acting at the ends of the muscle by the local cross-sectional area. However, in sheets such as those used here the situation is more complex. In order to calculate the stresses acting on the central region, one must assume that (1) the specimen is of uniform thickness and (2) the force applied at the edge is uniformly distributed along the edge. We made every attempt to use specimens that were of uniform thickness. Obviously, there could have been local non-homogeneous areas but we feel that our methodology provided a reasonable upper limit to specimen non-uniformity of about 10 %. Assuming the worst non-homogeneity of a discrete change in thickness of 10 % at the central region, specimens of the size used would underestimate by 9·1 % or over-estimate by 8·8 % the stress in the central region if it were 10 % thinner or thicker, respectively, than the remainder of the specimen. We feel that the use of the support needles avoids stress concentrations and tearing of the tissue that are present with use of either individual hooks or strands of thread piercing the tissue.

Our assessment of fibre and cross-fibre anisotropy is dependent upon the presence of a predominant orientation of fibres in the specimen. The fibre angle gradient is quite steep near the endocardial and epicardial surfaces (Streeter *et al.* 1979). However, in the regions where we selected our specimens, the gradient of fibre angle over a 2 mm thick specimen would be expected to be about 15°. By direct measurement of the fibre angles of the two cut surfaces, we verified that there was no more than a 10–15° difference in fibre angles. Thus, we can speak of a predominant fibre direction in each specimen. This not only enables us to assess the intrinsic anisotropy of muscle fibres but also enables us to load the specimen along its principal axes (i.e. parallel and perpendicular to the fibres). This simplifies both the experimental and analytical methodology since shear strains and stresses can be avoided. In some specimens with pronounced anisotropy, the initial square target was deformed into a rectangular shape but visual inspection of the target on the video monitors verified the absence of shear strains since in no case did we see distortion of the square into a parallelepiped.

One of the primary goals of this study was to compare biaxial muscle properties in and perpendicular to the predominant fibre direction in a sheet of muscle. The specimens we used were probably suited for this purpose. Taking a partial thickness slice of the ventricular wall certainly does not enable one to ascertain the three-dimenional properties of the tissue. It is likely that the full thickness tissue is stiffer than that measured in the slice since the constraints in the transverse direction between layers have been removed by the slicing. In addition, there are unknown numbers of transversely oriented fibres that have been cut. The quantitative

influence of these factors cannot be determined from our experimental methodology. Short of actually performing a full three-dimensional test on a specimen with uniformly oriented fibres, however, even the specific influence of removing the transverse constraints by slicing the tissue is difficult to determine.

As in all *in vitro* muscle tests, viability of the specimen is of concern. Even though we were interested in assessing only the passive muscle properties, in which case viability may not be as crucial as in active muscle; some assessment of tissue viability is still important. We did not observe any evidence of contracture as evidenced by a continuously rising unstretched force in any of the specimens. In addition, when some specimens were transiently warmed to 37 °C many would begin to manifest spontaneous contractions that would cease upon cooling the specimen to the test temperature of 30 °C.

Finally, some mention should be made of quantification of the results. As stated earlier, the goal of studies of this nature is to arrive at a concise yet still complete description of the constitutive relations of the material. For non-linear, anisotropic materials this description could take the form of a strain energy function which is non-linear in the strain components. For example Tong & Fung (1976) proposed an exponential strain–energy function for skin and vascular tissue while others prefer an incremental polynomial strain–energy function (Patel, Janicki, Vaishnav & Young, 1973) or a high-order polynomial approach (Blatz, Chu & Wayland, 1969). Each method has its advantages and drawbacks and it is not clear which method is more suitable for describing myocardial tissue because of insufficient data to date. Formulation of such a relationship, while extremely important for further progress, is beyond the scope of this present paper.

The qualitative comparisons described here suffice for determination of the presence or absence of anisotropy, heterogeneity, and differences between uniaxial and biaxial tests, even though the full constitutive relations have not been derived. Nevertheless, the results are of interest in that they are the first descriptions, to our knowledge, of myocardial properties under well controlled and accurately measured direct, multiaxial loading conditions. In subsquent studies that will be conducted on an improved apparatus, we hope to be able to obtain more quantitative results.

Implications of the results

The results of this study demonstrate that myocardial tissue under biaxial loading conditions exhibits highly non-linear elasticity as well as viscoelasticity. These are also characteristics seen in uniaxial tests (Pinto & Fung, 1973; Weisfeldt, Loeven & Shock, 1971; Little, 1976; Spurgeon, Thorne, Yin, Shock & Weisfeldt, 1977) and biaxial tests in skin (Lanir & Fung, 1974), and vascular tissue (Manak, 1980). The rather small degree of strain-rate dependence (Fig. 3), together with the relative constancy of the area enclosed by the hysteresis loop over a 100-fold strain-rate range, suggest that the tissue is non-linearly viscoelastic. Only when an appropriate constitutive relation has been formulated, however, will we be able to quantitatively and adequately address the complex problem of describing the non-linear viscoelastic behaviour of cardiac tissue.

There can be markedly different results in the same specimen (Figs. 4 and 5) when comparing biaxial with our uniaxial tests, which are also referred to as 'strip biaxial

tests' (Fung, 1973*a*) and are analogous to the conditions in papillary muscle tests. These results show that tissue under biaxial loading is stiffer than under uniaxial loading. Hence, it is quite likely that our current estimates of the wall stresses acting in the intact heart, which have been almost exclusively calculated from uniaxial test data (Gould, Ghista, Brombolich & Mirsky, 1972; Janz & Grimm, 1972; Pao, Ritman & Wood, 1974; Panda & Natarajan, 1977), are underestimations of the true stresses. In addition, like the unconstrained uniaxial condition it is clear that erroneous conclusions may be reached when one performs two sequential constrained uniaxial tests in an attempt to deduce biaxial behaviour. Only a true biaxial test is a reliable means of ascertaining the muscle properties.

The biaxial test results clearly show the presence of the long-suspected anisotropy of cardiac tissue even in the passive state. Anisotropy between fibre and cross-fibre directions has implications both for our interpretation of intact heart mechanics as well as for our understanding of the structural–functional interrelationships of the wall. Our findings suggest that measurements of relative deformations across the wall of the heart may reflect more the variation of fibre angle across the wall (Streeter *et al.* 1969; Arts & Heneman, 1980; Rabinowitz, 1978) than any intrinsic anisotropy of the entire wall (Olsen *et al.* 1981; Rabinowitz, 1978). Whether or not the anisotropy within a fibre layer is manifest as anisotropy of the entire wall depends upon a multitude of factors, including (1) how the layers are tethered to one another, (2) the variation of fibre angles among the layers, (3) the local forces acting upon each layer and (4) the regional differences in the presence and directionality of the anisotropy which our results indicate are present. With the demonstration of anisotropy as well as regional differences in myocardial anisotropy, it becomes evident that in order to achieve a precise understanding of regional three-dimensional cardiac mechanics even in the passive state one must obtain far more information than is available from closed-form solutions derived from simple geometric models. If one wishes to reach this level of understanding one must use approximate methods such as the finite-element model (Gould *et al.* 1972; Janz & Grimm, 1972; Pao *et al.* 1974; Bergel & Hunter, 1979; Vinson *et al.* 1979; Yin, 1981) that can account for the myriad of complexities present in the intact heart.

We have no data with which to speculate on the structural basis for the observed anisotropy. The tertiary structure of the myocardial fibre bundle and its collagenous and other fibrous or muscular interconnexions with adjoining structures certainly should influence the three-dimensional function (Borg, Ranson, Moslehy & Caulfield, 1981).

In summary, this study of sheets of canine myocardium under passive conditions subjected to biaxial and uniaxial loading has demonstrated the following: (1) there is anisotropy between the fibre and cross-fibre directions and some regional dependence to this anisotropy; (2) myocardium under biaxial loading exhibits both non-linear elasticity and viscoelasticity; (3) biaxial compared to uniaxial tests yield both quantitative as well as qualitative differences; (4) our current estimates of wall stresses in the intact heart may be erroneous since they are based upon uniaxial test data.

This work was supported in part by grant no. P-50 HL 17655 from the National Heart, Lung and Blood Institute, The National Institute of Health, Bethesda, MD, U.S.A. L. L. D. was supported in part by an award from the Medical Scientist Training Program and F. C. P. Y. was the recipient of a Frank T. McClure Fellowship from the Applied Physics Laboratory of the Johns Hopkins University.

REFERENCES

ARTS, T. & RENEMAN, R. S. (1980). Measurement of deformation of canine epicardium *in vivo* during cardiac cycle. *Am. J. Physiol.* **239**, H432–437.

BERGEL, D. A. & HUNTER, P. J. (1979). The mechanics of the heart. In *Quantitative Cardiovascular Studies*, ed. HWANG, N. H. C., GROSS, D. R. & PATEL, D. J. Baltimore: University Park Press.

BLATZ, P. J., CHU, B. M. & WAYLAND, H. (1969). On the mechanical behavior of animal tissue. *Trans. Soc. Rheol.* **13**, 83–102.

BORG, T. K., RANSON, W. F., MOSLEHY, F. A. & CAULFIELD, J. B. (1981). Structural basis of left ventricular stiffness. *Lab. Invest.* **44**, 49–54.

DIXON, W. J. (ed.) (1981). *B.M.D.P. Statistical Software*. Los Angeles: University of California Press.

FUNG, Y. C. (1967). Elasticity of soft tissues in simple elongation. *Am. J. Physiol.* **213**, 1532–1544.

FUNG, Y. C. (1973*a*). Biorheology of soft tissues. *Biorheology* **10**, 139–155.

FUNG, Y. C. (1973*b*). Biomechanics, its scope, history, and some problems of continuum mechanics in physiology. *Appl. Mech. Rev.* **21**, 1–20.

GOULD, P., GHISTA, D., BROMBOLICH, L. & MIRSKY, I. (1972). *In vivo* stresses in the human left ventricular wall: analysis accounting for the irregular three-dimensional geometry and comparison with idealized geometry analysis. *J. Biomech.* **5**, 521–539.

GREEN, A. E. & ADKINS, J. E. (1960). *Large Elastic Deformations and Nonlinear Continuum Mechanics*. Oxford: Clarendon.

HUISMAN, R. M., ELZINGA, G., WESTERHOF, N. & SIPKEMA, P. (1980). Measurement of left ventricular wall stress. *Cardiovascular Res.* **14**, 142–153.

HUNTSMAN, L. L., DAY, S. R. & STEWART, D. K. (1977). Non-uniform contraction in the isolated cat papillary muscle. *Am. J. Physiol.* **233**, H613–616.

JANZ, R. F. & GRIMM, A. F. (1972). Finite element model for the mechanical behavior of the left ventricle: prediction of deformation in the potassium-arrested heart. *Circulation Res.* **30**, 244–252.

KRUEGER, J. W. & POLLACK, G. H. (1975). Myocardial sarcomere dynamics during isometric contraction. *J. Physiol.* **52**, 391–408.

LANIR, Y. & FUNG, Y. C. (1974). Two-dimensional mechanical properties of rabbit skin. II. Experimental results. *J. Biomech.* **7**, 171–182.

LITTLE, R. C. (1976). The effect of acute hypoxia on the viscoelastic properties of the myocardium. *Am. Heart J.* **92**, 609–614.

MANAK, J. J. (1980). The two-dimensional *in vitro* passive stress–strain relationships for the steer thoracic aorta blood vessel tissue. *J. Biomech.* **13**, 637–646.

MIRSKY, I. (1976). Assessment of passive, elastic stiffness of cardiac muscle: mathematical concepts, physiologic and clinical considerations, directions of future research. *Prog. cardiovasc. Dis.* **18**, 277–308.

MORIARTY, T. F. (1980). The law of Laplace: its limitations as a relation for diastolic pressure, volume, or wall stress of the left ventricle. *Circulation Res.* **46**, 321–331.

OLSEN, C. O., LEE, K. L., TYSON, G. S., MAIER, G. W., DAVIS, J. W., MCHALE, P. A. & RANKIN, J. S. (1981). Anisotropic mechanical properties of the left ventricle in the conscious dog. *Circulation Res.*, Suppl. IV, **64**, 174.

PANDA, S. C. & NATARAJAN, R. (1977). Finite-element method of stress analysis in the human left ventricular layered wall structure. *Med. biol. Engng & Comput.* **15**, 67–71.

PAO, Y. C., RITMAN, E. & WOOD, E. H. (1974). Finite-element analysis of left ventricular myocardial stresses. *J. Biomech.* **7**, 469–477.

PATEL, D. J., JANICKI, J. S., VAISHNAV, R. N. & YOUNG, J. T. (1973). Dynamic anisotropic viscoelastic properties of the aorta in living dogs. *Circulation Res.* **32**, 93–107.

PINTO, J. G. & FUNG, Y. C. (1973). Mechanical properties of the heart muscle in the passive state. *J. Biomech.* **6**, 597–616.

RABINOWITZ, S. A. (1978). Myocardial mechanics: constitutive properties and pumping performance of the infarcted ventricle. Ph.D. Dissertation, Harvard University, Cambridge, MA, U.S.A.

SPURGEON, H. A., THORNE, P. R., YIN, F. C. P., SHOCK, N. W. & WEISFELDT, M. L. (1977). Increased dynamic stiffness of trabeculae from senescent rats. *Am. J. Physiol.* **232**, H373–380.

STREETER, D. D., SPOTNITZ, H. M., PATEL, D. J., ROSS, J. JR & SONNENBLICK, E. H. (1969). Fiber orientation in the canine left ventricle during diastole and systole. *Circulation Res.* **24**, 339–347.

TONG, P. & FUNG, Y. C. (1976). The stress–strain relationship for the skin. *J. Biomech.* **9**, 649–657.

VINSON, C. A., GIBSON, D. G. & YETTRAM, A. L. (1979). Analysis of left ventricular behavior in diastole by means of finite-element method. *Br. Heart J.* **41**, 60–67.

WEISFELDT, M. L., LOEVEN, W. A. & SHOCK, N. W. (1971). Resting and active mechanical properties of trabeculae carnae from aged male rats. *Am. J. Physiol.* **220**, 1921–1927.

WIEGNER, A. & BING, O. (1979). Laser scanner measurement of central segment performance in isolated cardiac muscle preparations. *Am. J. Physiol.* **237**, H260–264.

YIN, F. C. P. (1981). Ventricular wall stress. *Circulation Res.* **49**, 829–842.

YIN, F. C. P., TOMPKINS, W. R., PETERSON, K. L. & INTAGLIETTA, M. (1972). A video-dimension analyzer. *IEEE Trans. bio-med. Eng.* **19**, 376–381.